ACS OMEGA

http://pubs.acs.org/journal/acsodf

Article

Dechlorination Apparatus for Treating Chloride Salt Wastes: System Evaluation and Scale-Up

Brian J. Riley,* Saehwa Chong, and Charmayne E. Lonergan

Cite This: *ACS Omega* 2021, 6, 32239−32252

Read Online

ACCESS | Metrics & More | Article Recommendations | Supporting Information

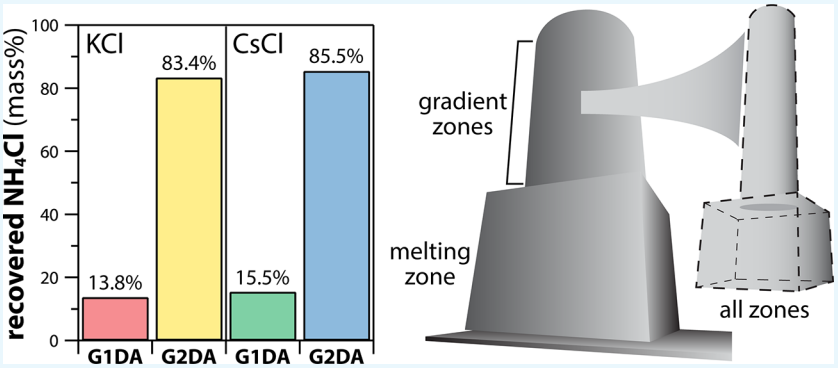

ABSTRACT: This paper describes an apparatus used to remove chlorine from chloride salt-based nuclear wastes from electrochemical reprocessing and/or chloride-based molten salt reactors (MSRs) through dechlorination by reacting the salts with ammonium dihydrogen phosphate ($NH_4H_2PO_4$ or ADP) at temperatures up to 600 °C to produce NH_4Cl as a byproduct. The benefits of removing the Cl from these salts include ^{37}Cl recovery from Cl-based MSR salts, formation of UCl_3 from the NH_4Cl, as well as removal of Cl from the salts and conversion of the salt cations to oxides to allow for immobilization in a chemically durable iron phosphate waste form. This generation-2 system is an improvement over the generation-1 system and provides a means for scaling up salt throughput as well as NH_4Cl recovery. The generation-2 system includes a five-zone furnace so the temperature of the four-zone gradient furnace can be tailored to control the location of NH_4Cl condensation on a four-piece fused quartz off-gas system. Both ADP and NH_4Cl decomposition reactions include the production of NH_3 and acids (i.e., H_3PO_4 and HCl, respectively), so careful temperature control is needed during the ADP-salt reactions to maximize the NH_4Cl production and minimize NH_4Cl decomposition. In two sets of experiments run in the generation-1 and generation-2 apparatuses, NH_4Cl yields were ≥5.5-fold higher for the new system compared to the original prototype system and the batch sizes can be ≥2.5-fold higher. In addition, some thermodynamic experiments evaluating the reactions of ADP + KCl as well as decomposition of pure NH_4Cl were performed to assess the temperatures of the reactions and identify off-gas products.

1. INTRODUCTION

Salt-based waste streams are generated through electrochemical reprocessing of used nuclear fuel and from decommissioning of molten salt reactors (MSRs). While electrochemical reprocessing is usually performed with chloride-based salts (e.g., LiCl-KCl eutectic),[1] MSR designs often utilize either chloride-based or fluoride-based salts in a salt coolant + solid fuel design (1-salt) or in a dual salt coolant/fuel (2-salt) configuration.[2,3] In both electrochemical reprocessing and MSRs, as fission products build up into the salts over time, the efficiencies of these processes diminish. At some point, the salts will require direct immobilization in a high-level waste salt repository or treatment for immobilization into an environmentally stable waste form.

Very few waste form options exist that have high halide loadings and good chemical durability. To complicate this, some of the more promising options are not easy to produce, adding costs associated with implementation in a real-world application. Some examples of potential waste forms are glass-bonded ceramics such as sodalite [e.g., $Na_8(AlSiO_4)_6Cl_2$][4−7] and apatite [e.g., $Ca_5(PO_4)_3Cl$, $Ca_5(PO_4)_3F$, and $Pb_{9.85}(VO_4)_6I_{1.7}$].[4,8−10] Glasses that can accommodate high fractions of halides while also remaining chemically durable are very limited and include lead tellurite glass for rare-earth (RE) chlorides[11] and Bi_2O_3-Ag_2O-based tellurite glass for iodine immobilization.[12]

Received: September 13, 2021
Accepted: November 4, 2021
Published: November 16, 2021

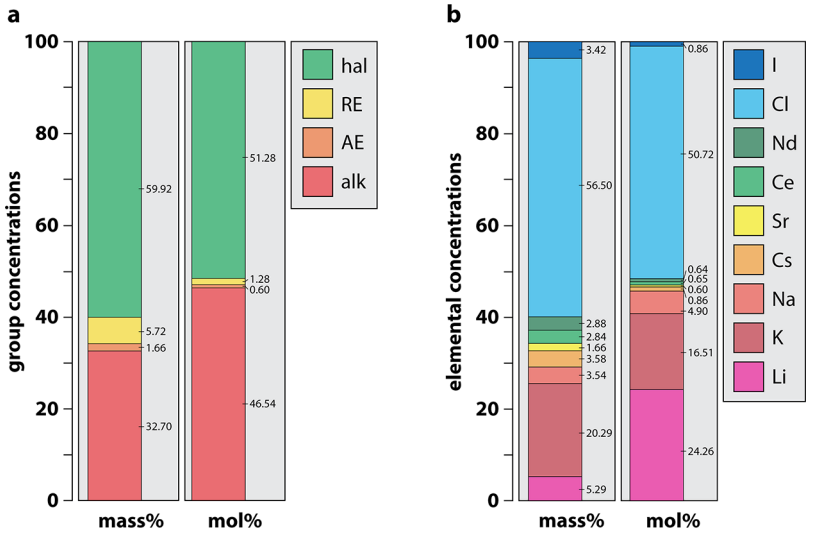

Figure 1. Comparison of mass % and mol % distributions for an ERV2 electrochemical reprocessing salt simulant[14] (a) by group (hal = halides; RE = rare earths; AE = alkaline earths; alk = alkali) and (b) by element.

An alternative approach to direct immobilization of the salt into a single waste form is to partition the salt.[13] First, the ideas discussed henceforth assume some fraction of (or complete) actinide recovery so that little (or no) burnable fuel constituents are left in the salt for subsequent steps. Second, since one of the main limitations of waste form fabrication is working with halides, removing these halides up front opens up additional options for waste form fabrication. For salt processing applications where the anions associated with the cations are halides, the halides will comprise >50 mol % of the salt constituents, especially as fission products are generated; this is illustrated in Figure 1 showing an example of an electrochemical salt simulant used in a previous study (i.e., ERV2).[14] Removing this fraction is beneficial from several perspectives. If the initial chloride salt (before being subjected to fission products) contained any natural ^{35}Cl, then some can be activated by thermal neutrons to ^{36}Cl, a long-lived radioisotope ($t_{1/2}$ = 3.01 × 10^5 years) contributing to repository dose calculations. This can be avoided if the Cl (i.e., ^{35}Cl + ^{36}Cl) is recovered and recycled. This activation issue can be reduced if initial salts are enriched in ^{37}Cl. For F-containing salts, the fluorine could likely be discarded if recycling was not desired.

Demonstrated options for dechlorinating these types of salt wastes include the silica aluminophosphate (SAP) process whereby Cl is removed as HCl and the resulting product is immobilized in a dense waste form,[15,16] reacting ultrastable H-Y zeolite (USHYZ) with chloride salts where HCl is evolved followed by immobilization in a waste form,[17,18] and removing Cl as NH_4Cl through reactions with ammonium hydrogen phosphates [e.g., $NH_4H_2PO_4$ also called ADP, $(NH_4)_2HPO_4$].[14] It is likely that some of these processes could also be implemented for defluorinating fluoride-based MSR wastes. Finally, removing the halides and converting the remaining salt cations to other forms (e.g., oxides, phosphates) opens up waste form options to more well-studied candidates such as borosilicate glass,[19,20] phosphate glass,[21,22] and/or monazite-based (i.e., $REPO_4$)[23−25] materials for RE elements.

In the current work, a new system called the generation-2 dechlorination apparatus (G2DA) was designed and tested for dechlorinating chloride-based salts for immobilization of the salt cations in iron phosphate glass. The implemented design is a concept based off a prototype system called the generation-1 dechlorination apparatus (G1DA) documented in detail elsewhere (see Figure S2, Supporting Information)[14] but with several modifications and upgrades. Some high-level details of the G1DA are presented in this paper and in the Supporting Information. Here, chloride-based salts are reacted with ADP, the Cl is removed in the form of a volatile product (i.e., NH_4Cl) that can be condensed and captured/recovered, and the alkali-rich phosphate melt can be reacted with glass-forming components (e.g., Fe_2O_3) to tailor the final properties of the vitrified product. The concept of dehalogenating chloride salts using phosphates is not a new idea,[15,26−28] but in this paper, we describe the new apparatus in detail. Additional thoughts are provided for how this type of system could be scaled-up for a continuous processing approach versus a batch process. The process flow diagram for this system is provided in Figure S1 (Supporting Information).

During dechlorination, ADP can break down into NH_3 and H_3PO_4 [reaction 1],[29] H_3PO_4 can break down into P_2O_5 and H_2O [reaction 2],[29] and NH_4Cl can decompose into NH_3 and HCl [reaction 3][30] so the full recovery of NH_4Cl is complicated; note that "*s*" denotes solid, "*l*" denotes liquid, and "*v*" denotes volatilized product (these reactions require heat, hence the use of Δ). Complex control of the heating rates, heating hold temperatures, and off-gas system temperatures is required to achieve full recovery of the NH_4Cl condensates.

$$NH_4H_2PO_{4(s)} \xrightarrow{\Delta} NH_{3(v)} + H_3PO_{4(l)} \quad (1)$$

$$2\,H_3PO_{4(l)} \xrightarrow{\Delta} P_2O_{5(l)} + 3\,H_2O_{(v)} \quad (2)$$

$$NH_4Cl_{(s)} \xrightarrow{\Delta} NH_{3(v)} + HCl_{(v)} \quad (3)$$

One benefit for acquiring the Cl as NH_4Cl is that, if so desired, it could be reacted with uranium metal (U^0) to create UCl_3, an oxidant that is used in an electrorefiner through reaction 4 shown below; UCl_4 can form as an unwanted byproduct (as it can lead to vessel corrosion) shown in reaction 5.[14,31] The ability to remove and recover Cl as NH_4Cl from the salt waste using this process is a benefit if the Cl is a

https://doi.org/10.1021/acsomega.1c05065
ACS Omega 2021, 6, 32239−32252

^{37}Cl-enriched material, but otherwise, this process is likely not cost-effective. The process flow diagram provided in Figure S1 (Supporting Information) shows how this portion of the process fits into the overall procedure.

$$2\,U^{0}_{(s)} + 6\,NH_4Cl_{(s)} \rightarrow 2\,UCl_3 + 6\,NH_{3(g)} + 3\,H_{2(g)} \quad (4)$$

$$2\,U^{0}_{(s)} + 8\,NH_4Cl_{(s)} \rightarrow 2\,UCl_4 + 8\,NH_{3(g)} + 4\,H_{2(g)} \quad (5)$$

It should be noted that NH_4Cl is a common industrial agent that includes condensation of the vapor at large scales. Thus, technologies are already in place to implement NH_4Cl capture at an industrial scale and this could help with future developments. Also, NH_4Cl is a very diverse compound used in a variety of industrial-scale processes from fertilizers (as a source of N) to medicine. The technology discussed herein has the potential to push the waste loading limits of salt-based wastes to new limits that are unachievable by conventional approaches[13] such as the glass-bonded sodalite waste form,[7] the USHYZ process,[32] or tellurite glass.[33]

2. SYSTEM DESIGN

Parameters and details of the G1DA and the G2DA as well as accompanying equipment are provided in Table 1 and can be referenced throughout this section. This includes both similarities and differences between the systems.

2.1. Generation-1 Dechlorination Apparatus. The G1DA used for prototype experiments is shown in Figure S2 (Supporting Information). This system utilized a box furnace (Thermolyne). A small 32 mm hole in the top of the furnace is where the off-gas glassware exited the system, which comprised custom-made pieces of GE-214 fused quartz of different sizes and wall thicknesses (details provided in Figures S2 and S11, Supporting Information). The region between the top of the hot zone inside the furnace and the top of the furnace exterior was insulated, which led to a drastic temperature drop inside the snorkel extension piece of the off-gas glassware (see Figure S2, Supporting Information, for more details). The system was designed for operation with 100 mL high-form 99.8% alumina crucibles (ACA3710; McDanel Advanced Ceramic Technologies; Beaver Falls, PA).

2.2. Generation-2 Dechlorination Apparatus. The G2DA design schematic is presented in Figure 2, and pictures are presented in Figure 3. The system, built by Deltech Inc., has five separately heated zones, each with two sets of coil elements. All of the zones have independent temperature control capability provided by Eurotherm 2416 setpoint controllers protected by WEST 6700+ overtemperature controllers (see Figure 3c). Figure 2 shows the different components of the system, how these components are arranged, and an example of a 250 mL conical alumina crucible (ACC3742; McDanel Advanced Ceramic Technologies) used in the current study (Figure 2f). All of the glassware for the system was designed by our team and custom-built by GM-Quartz (Oakland, CA) out of GE-214 fused quartz. Wider crucibles could also be implemented if needed, but this could require a different piece of glassware (see Figure 2c-3) to fully cover the crucible and help prevent NH_4Cl vapors from leaking into the furnace between the joint of the crucible and glassware. Other views of the G2DA at different orientations and showing other components are provided in Figure 3 and Figures S3, S7, and S8 (Supporting Information). The water cooling was set up in series to cool the right condenser before the left one, where both are filled from the bottom ports and exit on the top ports, with a water setpoint temperature of 10 °C.

Table 1. Comparison of Generation-1 Dechlorination Apparatus (G1DA) and Generation-2 Dechlorination Apparatus (G2DA) Including Both Similarities and Differences

system	G1DA	G2DA
furnace dimensions of heatable zone ($D \times W \times H$; cm)[a]	15.8 × 13.1 × 10.3	12.7 × 12.7 × 12.7
furnace electrical ($V/A/W$)[b]	120/8.3/1000	208/20/5000
furnace temperature capability	∼1150 °C	∼1150 °C
insulated region between the primary furnace and off-gas system	6 cm	5 cm
temperature controllers[c]	(1×) Eurotherm 2416 (SP)	(5×) Eurotherm 2416 (SP) (5×) West 6700+ (OT)
type of off-gas heating capability	external (tapes and pads)	internal (all integrated into the four-zone gradient furnace)
off-gas glassware	all fused quartz to condensers	all fused quartz to condensers
separate pieces for off-gas glassware (excluding condensers)	3	4
crucible size capabilities (off-the-shelf)[d]	100 mL	≥250 mL
snorkel (ID × OD; cm)[e]	6.8 × 7.4	8.9 × 9.5
snorkel extension (ID × OD; cm)	2.8 × 3.2	3.8 × 4.2
condenser system	(2×) Friedrich system	(2×) Allihn system
condenser dimensions ($H \times$ OD; cm)	32.4 × 5.1	40.6 × 4.0
glassware fittings	ground glass (press-fit)	standard tapered glass joints (i.e., 24/40 or 50/50)

[a]D = depth, W = width, H = height. [b]V = volts, A = amperes, W = watts. [c]SP = setpoint, OT = overtemperature. [d]In both cases, custom crucibles could be made with similar heights but larger diameters to accommodate processing larger sample volumes. [e]ID = inner diameter, OD = outer diameter.

The jumper tube (Figure 2b) between the snorkel (Figure 2c-3) and the right Allihn condenser is comprised of GE-214 fused quartz. The design used on this jumper piece was intended to meet a few different needs: (1) the 10 cm height on the right side provided flexibility for differently sized crucibles to be used with the same off-gas glassware (allowing for height adjustments inside the furnace), (2) a wide throw (∼25.4 cm) provided clearance between the furnace placement and the location of the condenser system, and (3) the downward slope on the left allowed for gravity-assisted liquid condensate movement toward the right Allihn condenser. The platform placed under the furnace raised the system high enough upward to accommodate for the increased condenser height using the Allihn system versus the shorter Friedrichs condensers. Shorter (i.e., smaller volume) collection flasks can be utilized as needed to accommodate for shorter crucibles in the furnace if so desired.

2.3. Comparison of Generation-1 and Generation-2 Systems. Several things were changed between the G1DA and the G2DA, which included (1) the furnace (including both the size and opening design), (2) the off-gas system design, (3) the temperature control capability, (4) the type of glassware joints

https://doi.org/10.1021/acsomega.1c05065
ACS Omega 2021, 6, 32239−32252

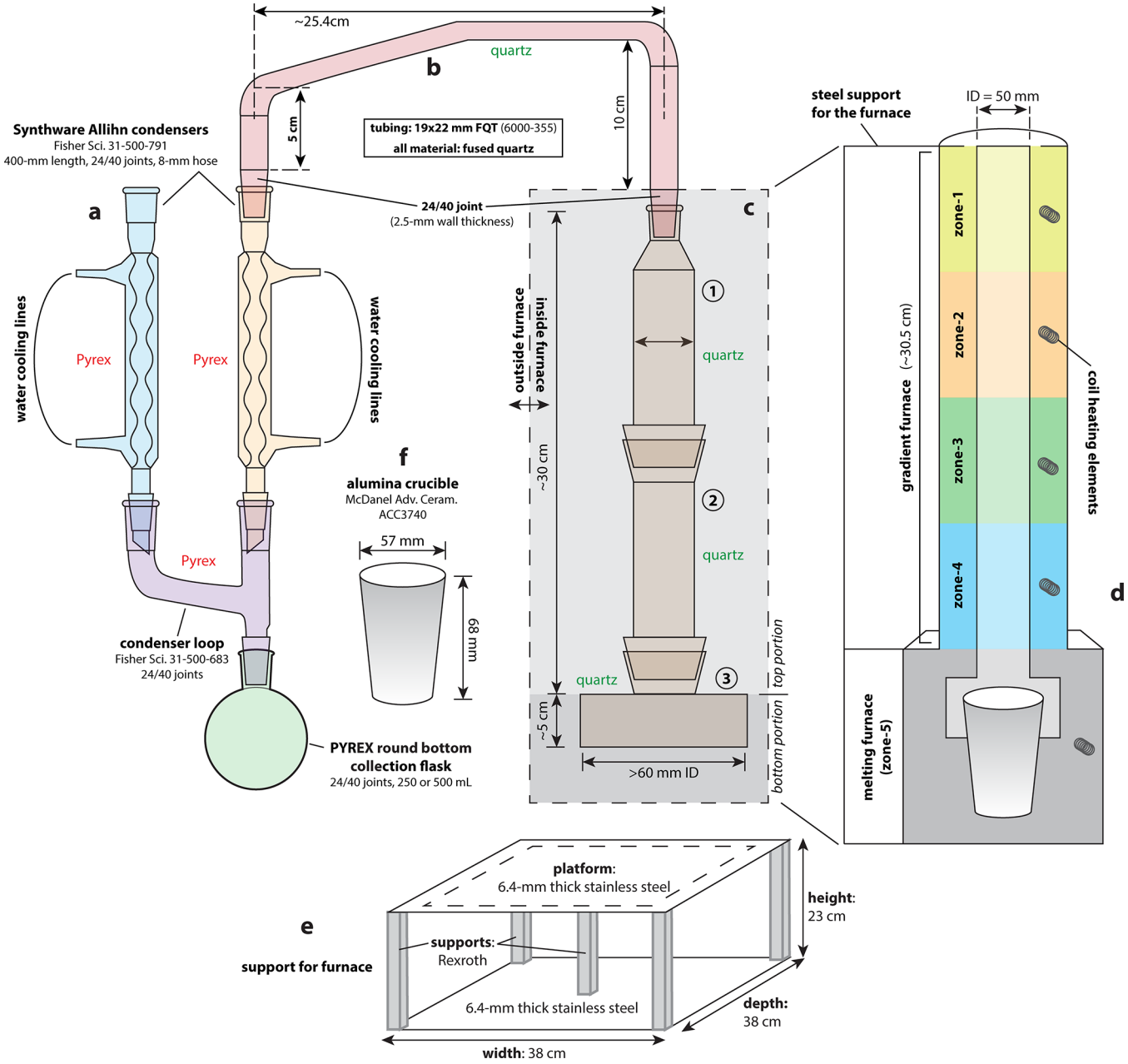

Figure 2. Schematic of the generation-2 dechlorination apparatus showing the (a) dual Allihn condenser system, (b) jumper piece between the condensers and the furnace glassware, (c) furnace with off-gas glassware (circled numbers are different pieces of glassware discussed in the text), (d) more detailed view of the furnace showing all five separately heated zones, (e) support for the furnace, and (f) 250 mL alumina crucible for holding the reactants. The drawings are not to scale.

used, and (5) the condenser system. The throughput limitations with the G1DA revolved around the smaller furnace size and how it was difficult to insert the crucible into the furnace with the snorkel on top (the top of the snorkel was inserted into the hole on the top of the furnace from underneath). This meant that the crucible size was restricted to what would fit into the furnace with the snorkel on top since they had to be inserted into the furnace together. The G2DA can easily accommodate a 250 mL conical crucible and much wider, higher-volume crucibles if a larger-diameter snorkel were used. Also, the G2DA has two opening mechanisms where the front panel can be opened and/or where the entire furnace can be opened like a vertical clamshell. This upgrade provides the ability to load the entire system at the same time, i.e., the charged crucible (Figure 2f) + piece-c1 (Figure 2c-1) + piece-c2 (Figure 2c-2) + piece-c3 (Figure 2c-3).

The off-gas system design in the G1DA utilized custom-built pieces of fused-quartz that did not fit tightly together, resulting in some leakage around the joints during operation. A primary problem was the loose-fitting joint between the "L" tube riser Friedrichs condenser-1 (see Figure S2, Supporting Information) where condensed liquids would sometimes leak. All of the glassware joints in the G2DA are standard tapered joints (i.e., 24/40 or 50/50) and fit tightly all around. Also, the diameter of the off-gas glassware in the G1DA was limited to the size that could be accommodated by the fixed hole size (32 mm) on the top of the Thermolyne box furnace; the inner diameter of the snorkel extension is 28 mm (see Figure S2,

https://doi.org/10.1021/acsomega.1c05065
ACS Omega 2021, 6, 32239−32252

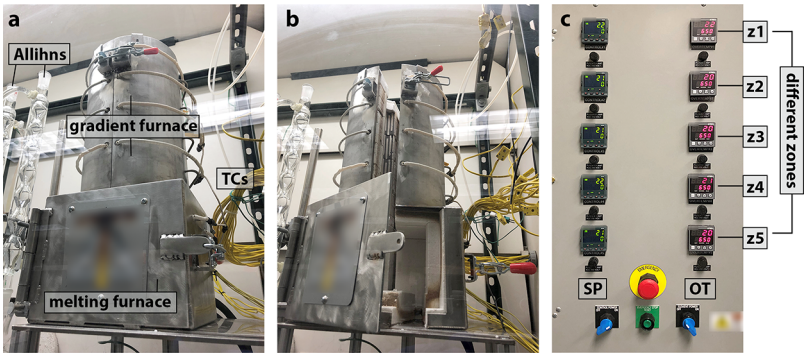

Figure 3. Pictures of the G2DA and components including (a) furnace while closed with the Type-K thermocouple (TC) bank for temperature monitoring shown to the right, (b) furnace while partially open (unlatched), and (c) furnace controller showing the different zones (i.e., z = zone) with five Eurotherm 2416 setpoint (SP) and five WEST 6700+ overtemperature (OT) controllers. The TC bank is connected to a data acquisition system outside the fumehood (not shown). Company logos have been blurred in the images.

Table 2. Targeted Batch and Final Glass Compositions of Experiments Performed in this Study[a]

	initial reactant chemicals					final glass components			
exp.	ADP (g)	Fe_2O_3 (g)	salt	salt (g)	NH_4^+/Cl^- (molar)	P_2O_5 (g)	Fe_2O_3 (g)	oxide	oxide (g)
G2DA Run-1	23.8165	10.8257	KCl	8.6606	1.782	14.6951	10.8257	K_2O	5.4713
G2DA Run-2	47.6334	21.6520	CsCl	17.3203	4.025	29.3902	21.6514	Cs_2O	14.4967
G1DA Run-1	23.8165	10.8257	KCl	8.6606	1.782	14.6951	10.8257	K_2O	5.4713
G1DA Run-2	23.8165	10.8257	CsCl	8.6606	4.025	14.6951	10.8257	Cs_2O	5.4713

[a]ADP = ammonium dihydrogen phosphate ($NH_4H_2PO_4$). Data are listed in mass except for the NH_4^+/Cl^- (molar ratio). Note that G1DA Run-1 and G1DA Run-2 are Simple-1 and Simple-6 from a previous study, respectively.[34]

Supporting Information). In nearly every experiment performed in the G1DA, some plugging of the snorkel was observed as a result of dendritic growth of NH_4Cl from the glassware surfaces inward toward the centerline. When plugging was observed, the excess NH_4Cl vapors would leak out of the small air gap between the top rim of the crucible and the snorkel (see Figure S2, Supporting Information). To prevent this plugging, a larger-diameter snorkel extension piece was needed in the redesigned system, so this was implemented in the G2DA where the minimum inner diameter of the off-gas system is 38 mm. Also, to allow for easier NH_4Cl condensate recovery, having more pieces in the off-gas system provided better access to these internal surfaces.

Better temperature control was needed in the G2DA for the off-gas system, so a four-zone gradient furnace was included in the new design. Due to the connectivity of the bottom hot zone (zone-4; Figure 2d) and the melting furnace (zone-5; Figure 2d), thermal diffusion from the melting furnace into the gradient furnace was unavoidable. This heat transfer was more evident as the setpoint temperature differences (ΔT) between the melting furnace and gradient furnace zones were larger (discussed in a later section). This heat leakage between the zones was actually desired to prevent the steep thermal drop off seen in the G1DA due to the insulation at the top of the Thermolyne box furnace. The goal of spreading out this thermal gradient over a larger vertical area was to also spread out the region where the NH_4Cl condensed, helping in preventing plugging the snorkel extension.

In the G2DA, all of the joints in the system are standard tapered joints. This helps prevent vapors from leaking during the heat-treatment process. Also, all of the joints are tapered in a downward fashion so that if leaking does occur, any liquids will drip back into place below.

Lastly, the condenser system implemented in the G2DA is based off a dual-Allihn system rather than the dual-Friedrichs system used with the G1DA and there are several differences between these two condenser types. The Allihn condensers are longer (400 mm) than the Friedrichs condensers and have a less tortuous pathway for internal gas flow. This makes the Allihn condensers easier to clean of solid condensates. Also, the inner diameter of the Allihns is smaller, so the cooled surface area is smaller. Also, the Allihns are externally cooled rather than internally cooled, which is part of why the cleaning is easier.

3. METHODS

3.1. Temperature Testing and Furnace Profiling. To evaluate the thermal tolerances of the furnace zones, several different heat treatments were performed with isothermal holds in the gradient furnace while the melting furnace was held at 600 °C, the typical maximum operating temperature for dechlorination. Based on the limitations of the Eurotherm 2416 controllers for these different furnace zones, the number of programmable segments was limited. Thus, a low-temperature test (T = 100, 150, and 175 °C) was run as well as a higher-temperature test (T = 200, 250, and 300 °C).

For these tests, the top of the furnace where the glassware exited was insulated with Kaowool to help prevent heat loss. Also, the Type-K TCs (Omega Engineering) were connected to a separate quartz tube that was placed down the interior of the empty off-gas glassware and resided in the bottom of an empty 250 mL alumina crucible.

3.2. Sample Compositions, Batching, and Sample Preparations. *3.2.1. Experiments Performed Using the G2DA.* Two samples were produced in this study with compositions presented in Table 2, which are called Run-1 where the salt was KCl (≥99%, 793590-1KG; Sigma Aldrich)

https://doi.org/10.1021/acsomega.1c05065
ACS Omega 2021, 6, 32239−32252

and Run-2 where the salt was CsCl (99.99%, 87640; Alfa Aesar). Run-1 and Run-2 were performed separately from one another with different target masses with simplified reactions shown in reactions 6 and 7, respectively, for a 1:1 molar ratio of salt to ADP, which was not the case in either reaction. It was expected that the unreacted ADP would thermally convert to P_2O_5, which is implied as a combined product between reactions 1 and 2.

$$2\,KCl_{(s)} + 2\,NH_4H_2PO_{4(l)} \vec{\Delta} 2\,NH_4Cl_{(v)} + 2\,H_2O_{(v)} + P_2O_5{:}\ K_2O_{(l)} \quad (6)$$

$$2\,CsCl_{(s)} + 2\,NH_4H_2PO_{4(l)} \vec{\Delta} 2\,NH_4Cl_{(v)} + 2\,H_2O_{(v)} + P_2O_5{:}\ Cs_2O_{(l)} \quad (7)$$

For both experiments, the target mass ratios of ADP:-Fe_2O_3:salt were 55:25:20 based on the DPF-5 glass formulation from our previous works,[13,14] which showed good chemical durability.[35−37] However, the experiments in the current work were run with simplified single-salt compositions instead of the more complex simulants such as ERV2 and ER(SF) termed Simple-1 (KCl) and Simple-6 (CsCl);[34] more details on the Simple formulations will be discussed in a follow-up publication. Each experiment was performed in two steps, which included (step-1) dechlorination using the Deltech G2DA and (step-2) vitrification using a separate high-temperature Deltech furnace. Chemicals were weighed on a four-place balance (ME204E; Mettler Toledo; 220 g maximum mass) and the heavier pieces, which included the crucible and all of the off-gas glassware, were weighed on a two-place balance (PL1502E; Mettler Toledo; 1520 g maximum mass). The masses of the crucible and the off-gas glassware were taken so that mass balances could be tracked.

For the dechlorination step, the salt was weighed and added to a 250 mL 99.8% alumina conical crucible (ACC3742; McDanel Advanced Ceramic Technologies) and this was followed by ADP (≥98.5%, Sigma Aldrich). The powders were mixed with a metal spatula, and the crucible was placed into the melting chamber in the G2DA (see the bottom of Figures 2d and 3a,b). The off-gas glassware was placed on top of the crucible (see Figure 2c-3,d), and the furnace was closed. For Run-1 (KCl), Kaowool was added around the exit port at the top of the off-gas glassware where piece-c1 (Figure 2c-1) exited the gradient furnace to help prevent heat loss. This was not done for Run-2 to evaluate the change in the location of NH_4Cl condensation. The heating profile used in the melting furnace is shown in Figure S6b (Supporting Information) and all four gradient temperature zones were set to 150 °C. Following dechlorination, the white condensates were imaged and scraped off the glassware using a metal spatula and a razor blade.

For the vitrification step, Fe_2O_3 (2024-05; 100.3%; J.T. Baker) was added to the solidified product from the dechlorination step in the original crucible. Due to the thermal shock issue that is common with ceramic crucibles, it is preferred that a new crucible be used at this step, but it usually results in the loss of material on the crucible walls that cannot be easily removed; this leads to an off-stoichiometry batch. It is also preferred that these crucibles are not rapidly heated or cooled to help prevent this shock. Cracking can also be introduced through mismatches between the thermal expansion coefficient of the alumina and the glass once the glass has reacted with the crucible. Also, the alkali-phosphate product is hygroscopic at this stage and makes grinding, or homogenization of any type, difficult. Thus, the Fe_2O_3 is not mixed with the alkali-phosphate solid but rather it is just placed on top of the solid. The filled crucible was added to a high-temperature Deltech furnace with $MoSi_2$ elements at 1050 °C without a lid. Following ∼1 h, the crucible was removed from the furnace and the melt quenched on an Inconel plate. It should be noted that the alumina crucibles had small fractures that are likely due to the rapid heating as the filled crucibles were inserted directly into the 1050 °C furnace.

3.2.2. Experiments Performed Using the G1DA. Similar experiments to G2DA Run-1 and G2DA Run-2 above were performed in the G1DA in separate experiments referred to as G1DA Run-1 (Simple1-KCl) and G2DA Run-2 (Simple6-CsCl), respectively.[34] The same chemicals were used, but differences included 100 mL alumina crucibles instead of 250 mL crucibles, the heating profile was slower with 1 h dwells at 200, 300, and 400 °C (i.e., Figure S6a) as opposed to the 10 min dwells at these temperatures used for the G2DA experiments (i.e., Figure S6b), and different masses were used between Run-1 and Run-2 (for G2DA experiments, the masses were doubled for Run-2 with CsCl).

3.3. Sample Characterization. The condensates from dechlorination and glasses produced after each run were collected and analyzed with powder X-ray diffraction (XRD) on cylindrically shaped zero-background quartz holders (32 × 2.5 mm with 10 × 1 mm cavity; MTI Corporation; Richmond, CA) using a Bruker D8 Advance (Bruker AXS Inc., Madison, WI) with a Cu tube. Data were collected using a LynxEye position-sensitive detector with a collection window of 3° 2θ. Scans were collected from 10 to 70° 2θ at a step angle of 0.194° 2θ with a dwell time of 0.5 s per step. For NH_4Cl fitting, pattern 22141 from the Inorganic Crystal Structure Database was used.

3.4. Differential Scanning Calorimetry, Thermogravimetric Analysis, and Evolved Gas Analysis. Differential scanning calorimetry (DSC) and thermogravimetric analysis (TGA) were performed on the G2DA Run-1 mixture of ADP and KCl. This mixture was made fresh using the reactants used in the large-scale experiment and ground to a fine powder in a Diamonite mortar and pestle. During this experiment, evolved gas analysis (EGA) was also done, which included gas chromatography (GC) coupled to a mass spectrometer (MS). The system utilized for this was a Netzsch 449 F1 Jupiter instrument connected to an Agilent 7890A GC and Agilent 5975 single quadrupole MS. A sample mass of 21.1 mg was placed in an alumina crucible, and then that was placed onto the DSC sample stage without a lid.

The sample was heated at a rate of 5 °C min^{-1} from room temperature to 600 °C with 10 min holds at 200, 300, and 400 °C and a 1 h hold at 600 °C. Air was used as the purge and protective gas at constant flow rates of 20 and 40 mL min^{-1}, respectively. The evolved gases moved from the DSC chamber to the GC−MS using a heated transfer tube and helium as the carrier gas. The gases flowed through the GC sampling loop (250 μL) and were sampled every minute. The GC injector was set to splitless mode. The sampled aliquot was injected into the GC column (GS-CarbonPLOT, 30 m long and 320 μm inner diameter) and eluted with He gas, and the species separated by the column prior to entering the MS for analysis. The GC−MS system measured samples under a He

https://doi.org/10.1021/acsomega.1c05065
ACS Omega 2021, 6, 32239−32252

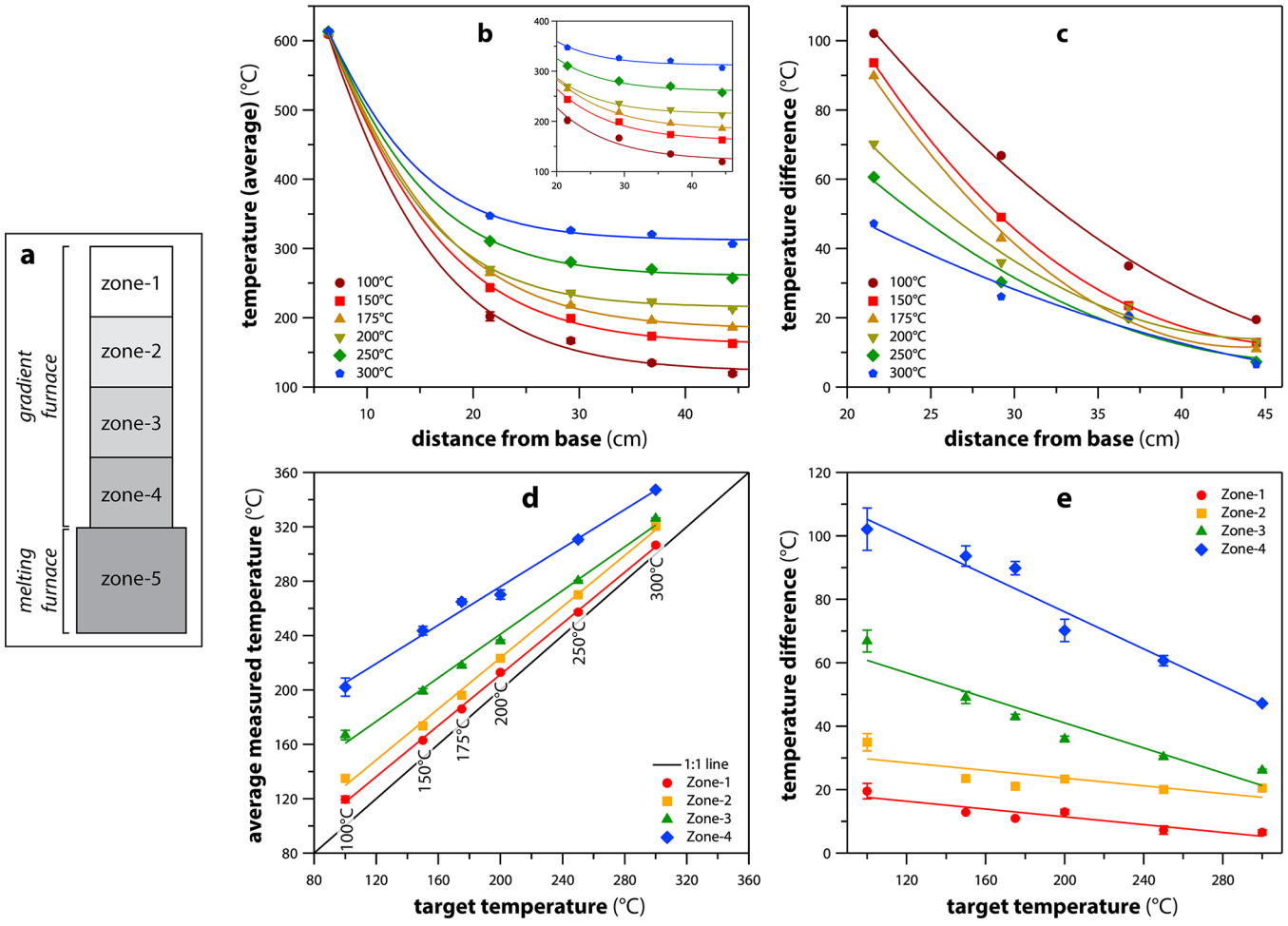

Figure 4. (a) Furnace zone layout. (b, c) Summary of temperature in the furnace as a function of distance from the base of the melting furnace at different setpoint temperatures including (b) average temperatures with fitted Sigmoid equations and (c) temperature differences (ΔT) of measured (T_{meas}) and targeted (T_{targ}) with polynomial fits to the data. (d) average temperatures for different setpoints within gradient zones (i.e., zone-1 → zone-4, with zone-5 T_{SP} = 600 °C) and (e) ΔT values vs target temperatures for gradient zones (i.e., zone-1 → zone-4).

atmosphere with a constant column flow rate of 1.5 mL min^{-1}. The heated system components (e.g., the transfer tubing, sampling loop valve box, and GC column) were set to temperatures greater than 100 °C to prevent possible condensation of gaseous species. The MS ionization energy was set to 20 eV, the scan range m/z (mass-to-charge ratio) was 10−200, and the GC−MS interface held at 280 °C.

In addition, a 16.4 mg sample of NH_4Cl, the collected condensate from the G2DA Run-1 experiment with ADP and KCl, was also analyzed with DSC-TGA-EGA. This run included a ramp from room temperature to 450 °C at 20 °C min^{-1} to evaluate the NH_4Cl decomposition process.

4. RESULTS AND DISCUSSION

4.1. Furnace Profiling. The thermal profile runs for the lower-temperature test (T = 100, 150, and 175 °C) and the higher-temperature test (T = 200, 250, and 300 °C) are presented in Figures S4 and S5, respectively. This was done so that precise TC locations could be recorded. More detailed information is provided in Figure 4. The data shown for the average measured temperatures followed a predictable trend (Figure 4d) with increasing target temperatures. Taking the locations inside the furnace as distances from the base of the melting furnace (or the bottom of the heated region), the average temperatures were plotted. These data were fit to Sigmoid equations of the format shown in eq 8, where α, β, δ, and ε are all variables defined in Table S1 (Supporting Information). This equation format fit well for all datasets corresponding to different setpoint temperatures. When looking at these data, it was apparent that the gradient furnace could be set up to span a fairly wide range of different temperatures just by keeping all zones setpoints at the same temperature due to heat transfer between zones. Having the gradient temperature capability in this system provides greater flexibility to span the condensation region as needed based on the NH_4Cl production rate and expected quantities from different compositions.

$$y = \alpha + \beta/[1 + \exp(-\{x - \delta\}/\varepsilon)] \quad (8)$$

4.2. Experimental Runs in the G2DA. Condensates were collected for Run-1 (KCl) and Run-2 (CsCl) experiments as shown in Figures S7 and S8 (Supporting Information), respectively. Following the dechlorination process, the off-gas glassware was removed from the furnace along with the crucible. Pictures of the glassware with condensates for Run-1 and Run-2 are shown in Figures S7 and S8 (Supporting Information), respectively. The white condensation was not observed in any measurable quantity more than 2−3 cm below

https://doi.org/10.1021/acsomega.1c05065
ACS Omega 2021, 6, 32239−32252

Table 3. Summary of Condensate Masses Recovered after Run-1 and Run-2 from Different System Components (See Figure 2 for References to Glassware Pieces)[a]

		Run-1 (KCl)			Run-2 (CsCl)		
vessel piece	reference	m_i (g)	m_f (g)	m_c (g)	m_i (g)	m_f (g)	m_c (g)
piece-C1	Figure 2c-1	153.31	157.38	4.07	153.32	156.03	2.71
piece-C2	Figure 2c-2	145.10	146.16	1.06	145.12	147.27	2.15
piece-C3	Figure 2c-3	95.64	95.65	0.01	95.84	95.66	−0.18
piece-B	Figure 2b				122.80	122.77	−0.03
crucible	Figure 2f			0.04			0.05

[a]The values of m_i, m_f, and m_c denote initial mass, final mass, and mass of condensate recovered, respectively. Blank values denote that the system component was not weighed.

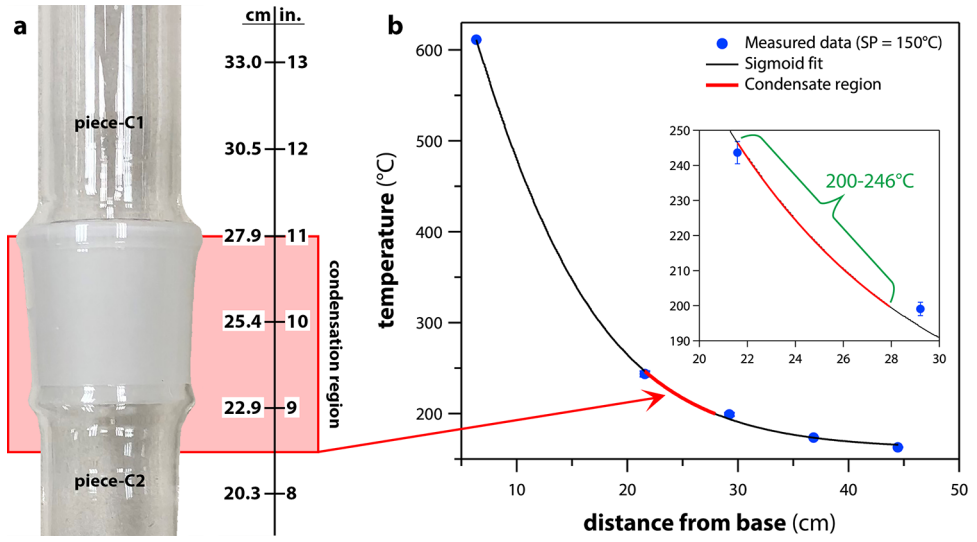

Figure 5. (a) Region where condensates were observed in the largest quantity showing piece-c1 and piece-c2 merged together at the tapered joint; a ruler is provided that shows the distances from the base of the melting furnace in both centimeters (cm) and inches (in.). (b) Plot showing the temperatures at these locations based on the Sigmoid fit (inset shows the relevant region magnified).

the upper joint of piece-c2 (Figure 2c-2), and a majority of the salt was condensed at the tapered joint between piece-c1 (Figure 2c-1) and piece-c2 (Figure 2c-2); masses of the different pieces are shown in Table 3. Slight mass losses documented in Table 3 could be due to moisture desorbed from the surfaces of the glassware. Since Run-1 was performed in the exact way the furnace was profiled, the condensate region equates to a temperature range (ΔT) of 200−246 °C as shown in Figure 5.

For Run-1, the condensates at the top of piece-c1 (Figure 2c-1) were slightly discolored (light brown), but otherwise, the rest of both condensates were very white and pure NH_4Cl based on XRD analysis shown in Figure 6; these data were refined using the Inorganic Crystal Structure Database Crystallographic Information File 20682 for NH_4Cl with the cubic space group $Pm\bar{3}m$.[38] The cause of the discoloration is unknown but assumed to be due to an impurity in the KCl based on the same discoloration in the crucible of Run-1 after dechlorination (not shown). The condensates can be observed to span nearly all of piece-c1 (Figure 2c-1) and approximately the top half of piece-c2 (Figure 2c-2) (see Figures S7 and S8, Supporting Information, for more details). The primary locations of condensates observed for Run-1 and Run-2 in the G2DA spanned 7.8−10.1 cm and 5.6−6.1 cm, respectively, compared to ∼3.1 cm observed in similar G1DA tests. This comparison helps quantify the differences in spread of the condensation region.

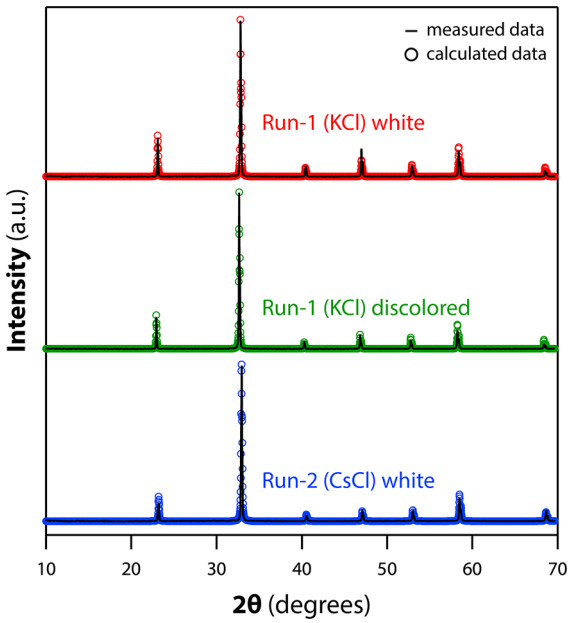

Figure 6. XRD data from NH_4Cl condensates from Run-1 (both white and discolored condensates) and Run-2. The phase match is NH_4Cl.

Figure 7 provides some comparisons of the NH_4Cl condensates recovered between the G1DA and G2DA

https://doi.org/10.1021/acsomega.1c05065
ACS Omega 2021, 6, 32239−32252

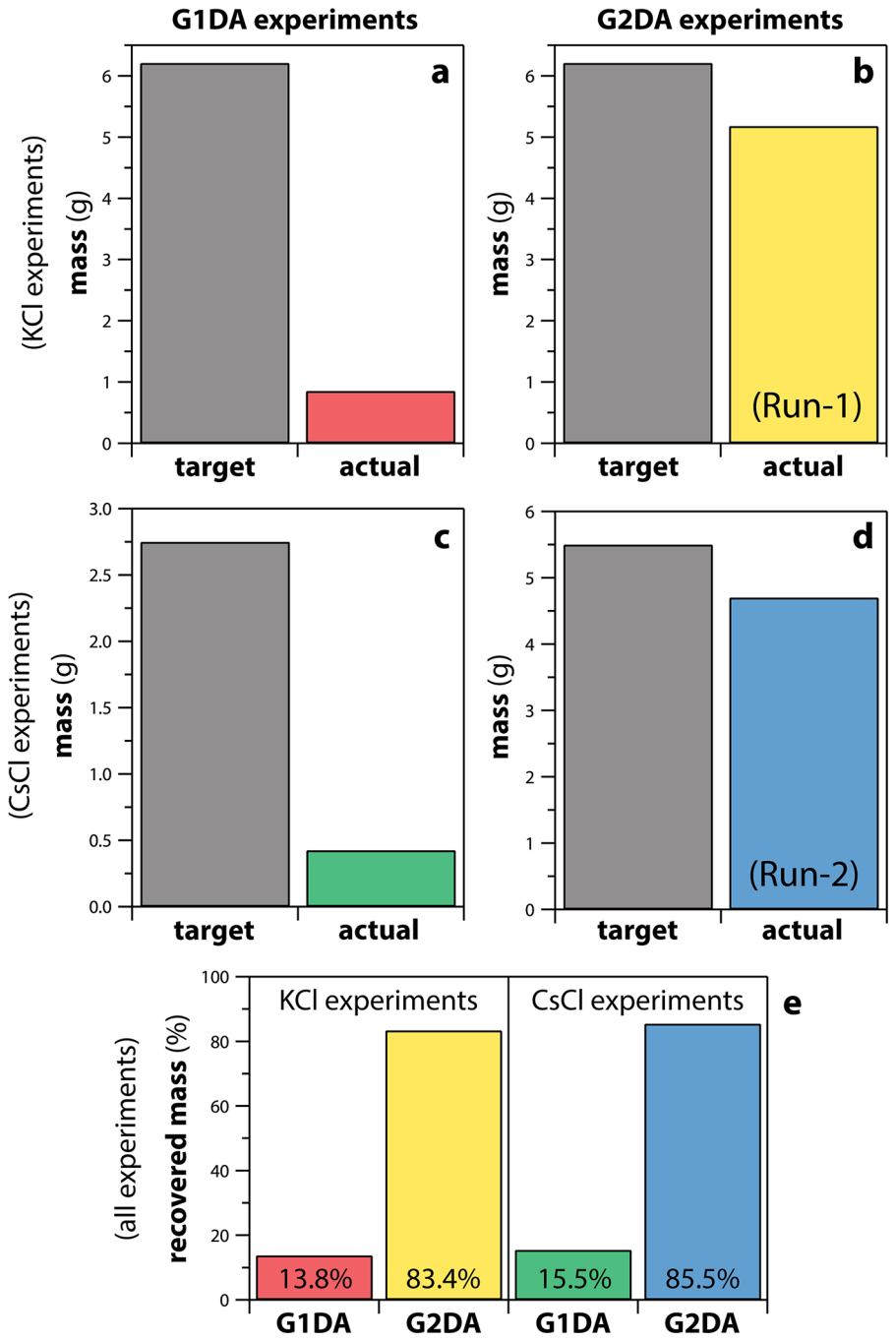

Figure 7. Comparison between NH_4Cl condensate mass recoveries during (a, b, e) KCl experiments and (c–e) CsCl experiments in (a, c, e) G1DA and (b, d, e) G2DA runs with (a–d) target values shown in gray; target values were calculated based on Cl as the limiting reagent in each experiment (see the NH_4^+/Cl^- ratio in Table 2). (e) Summary of the recovered masses (mass %) for all four experiments calculated based on expected recovery.

experiments. Both recoveries were very low for the G1DA experiments at 13.8 mass % for Run-1 and 15.5 mass % for Run-2, whereas the recoveries for both G2DA experiments were >80 mass % equating to 6.0×- and 5.5×-fold improvements, respectively (see Figure 7e). This is partly attributed to the off-gas glassware not plugging for either the G2DA experiment, which is in part due to the larger ID of the G2DA snorkel extension, but also due to the increased thermal gradient introduced by the gradient furnace. It should be noted that the volume of liquid present in the collection flask from each G2DA experiment was not measured, but it is possible that some of the NH_4Cl decomposed based on reaction 3 presented above, leading to NH_4Cl recoveries of <100 mass %.

Finally, the pHs of the liquid condensates present in the collection flask for G2DA Run-1 and G2DA Run-2 were 8 and 11, respectively; the Run-2 solution smelled of ammonia. The higher pH of the Run-2 solution is likely due to excess ammonia being produced during the ADP decomposition reaction shown in reaction 1 where any excess H_3PO_4 was converted to P_2O_5 before volatilizing [i.e., Reaction 2].

4.3. Vitrified Products from G2DA Dechlorination Runs. The vitrification steps for G2DA Run-1 and G2DA Run-

https://doi.org/10.1021/acsomega.1c05065
ACS Omega 2021, 6, 32239–32252

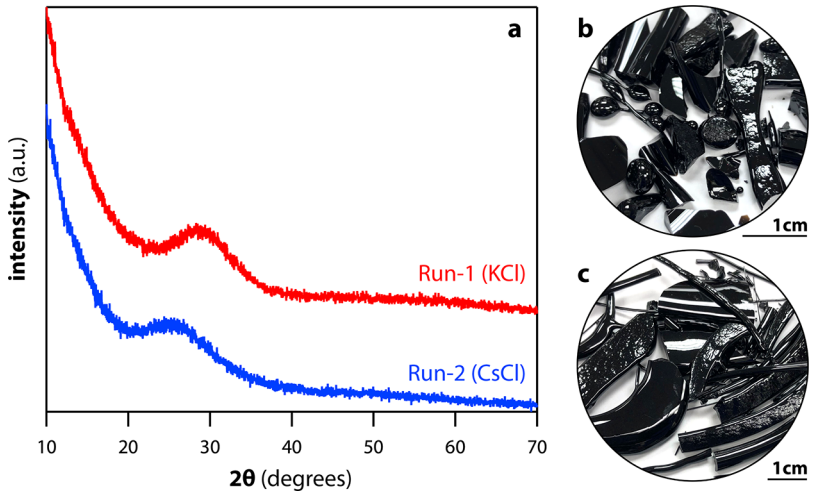

Figure 8. (a) XRD of quenched glasses from Run-1 (KCl) and Run-2 (CsCl) as well as pictures of quenched glasses after the vitrification processes of (b) KCl (Run-1) and (c) CsCl (Run-2) following dechlorination. Individual scale bars are shown for each picture.

2 produced similar outcomes where both glasses poured with low viscosity and resulted in dark black glasses (see Figure 8b and Figure 8c). The P-XRD data for both are presented in Figure 8a and show that both glasses were amorphous.

4.4. DSC-TGA-EGA on the ADP-KCl Mixture. The data from the DSC-TGA-EGA experiment on the ADP-KCl (G2DA Run-1) mixture is presented in Figure 9. As a reference, the melting temperature (T_m) of ADP is 190 °C and the sublimation point (T_{sp}) of NH_4Cl is 338 °C.[39] Based on the data from this mixture and the temperature callouts on endotherms in Figure 10b, the first peak (i.e., I) is the ADP melting event. The GC−MS peaks for NH_3 (Figure 9c) and H_2O (Figure 9d) indicate the decomposition of ADP based on reactions 1 and 2. The second endotherm (i.e., II) is possibly the melting of KCl in the H_3PO_4/P_2O_5 mixture due to the formation of a eutectic system as this is around the time where HCl is observed in the GC−MS scan in Figure 9e [see reaction 3]; note that pure H_3PO_4 boils at 407 °C and pure KCl melts at 771 °C.[39] The cause of the endotherm shown in (III) is unknown. The cause of the endotherm in (IV) is likely due to the sublimation, and likely the decomposition, of NH_4Cl since it coincides with HCl generation. It is unclear what the fifth endotherm is (i.e., V), but it seems to coincide with the largest peaks for H_2O and NH_3 evolution, so it could be due to additional ADP decomposition. These types of experiments are helpful for understanding the phosphate reactions, but even with simplified formulations such as ADP + KCl, it is difficult to distinguish between the different reactions occurring even with DSC-TGA-EGA. It does appear that the temperatures utilized during this heat-treatment process result in a fully dechlorinated salt as well as full decomposition of ADP. Also, the final mass of the sample based on the TGA data was around 65.8 mass % where the calculated final mass of P_2O_5-K_2O after full conversion to oxides should be around 62.1 mass %. If this mass discrepancy was due to undecomposed ADP, then this will fully decompose during the subsequent vitrification step.

The DSC-TGA-EGA data for the NH_4Cl experiment are shown in Figure 10. This data shows nearly full NH_4Cl decomposition, according to reaction 3, by the end of the experiment at ∼8 mass % left (based on TGA data).

5. CONSIDERATIONS FOR FUTURE DESIGNS

The G2DA was designed to meet the improvement needs identified during testing of the G1DA, but it is certainly not the most effective design for high-throughput processing and is not designed for continuous throughput processing. A horizontal orientation might be more efficient at performing the dechlorination process because the condensed NH_4Cl crystals cannot fall back into the crucible if they flake off the snorkel glassware. Having this horizontal orientation could also allow for a purge gas (e.g., air) to sweep the condensate away from the melting furnace, whereas if this was done in the vertical orientation, then the NH_4Cl condensates could fall back into the crucible or be transported to the condensers where recovery would be more difficult. One limitation to having a horizontal assembly is that the apparatus footprint would be much larger. The chosen design and footprint for the G2DA was based on available fumehood space. Between the furnace/stand, the condenser system, and the water chiller/circulator, the fumehood where this work is being conducted is already full. The horizontal system would work well in a walk-in style fumehood with a large horizontal footprint. This arrangement might also work well for scaling up the system for processing larger batches since a larger melting furnace could be implemented.

Neither the G1DA nor the G2DA utilized any sort of purge gas to drive condensates out of the furnace. The main reason for this is that purging would likely result in a thin layer of NH_4Cl across a larger surface, leading to more difficulty in harvesting the condensates. If so desired, it could be possible to draw all condensates through a liquid scrubber bed (e.g., NaOH) where any acidic gases (e.g., HCl) would be neutralized. This type of system could be introduced into future designs of the apparatus if so desired.

Another improvement would be to create a way to conduct the vitrification step in the same furnace as the dechlorination step. There are several reasons why this was not done in the G1DA and is not done in the G2DA described below.

First, the tops of both furnaces are open and finding a way to close these ports while the furnaces are energized would be difficult as both would require the removal of the off-gas glassware. Not removing the glassware before heating the furnace to higher temperatures would almost certainly result in

https://doi.org/10.1021/acsomega.1c05065
ACS Omega 2021, 6, 32239−32252

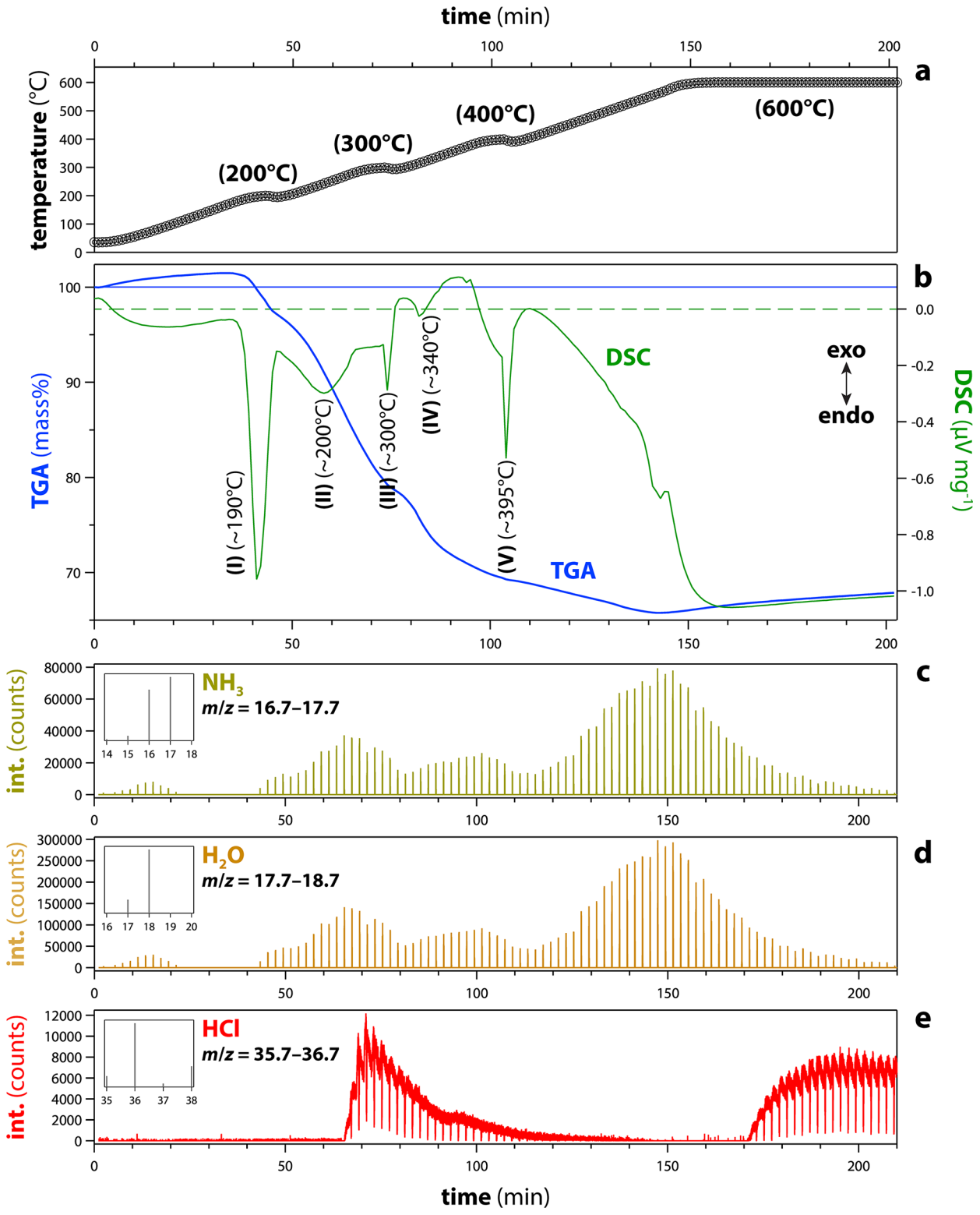

Figure 9. Summary of DSC-TGA-EGA data from the ADP-KCl experiment including (a) temperature vs time data, (b) DSC-TGA data, (c) GC−MS data for NH_3 (m/z = 16.7−17.7), (d) GC−MS data for H_2O (m/z = 17.7−18.7), and (e) GC−MS data for HCl (m/z = 35.7−36.7). The callouts in (b) are discussed in the text in more detail. The time on the GC−MS data is offset from the DSC-TGA data based on retention (delay) times. Insets on the GC−MS data show the mass spectra for each set of ions used to identify the species (i.e., intensity vs ion mass).

removal of the NH_4Cl. Also, the G2DA furnace cannot be easily opened without unlatching and opening the gradient furnace section. This is due to the way that the insulation seals the furnace and the electrical hazards of the exposed heating elements, deeming it unsafe to open while energized. Finding a way to plug the top of the furnace in an automated way (e.g., using a swing-style rotation mechanism) might be one way to plug the top of the furnace without opening it but again, this would require removing the off-gas glassware from the furnace while it is energized and at operating temperatures.

https://doi.org/10.1021/acsomega.1c05065
ACS Omega 2021, 6, 32239−32252

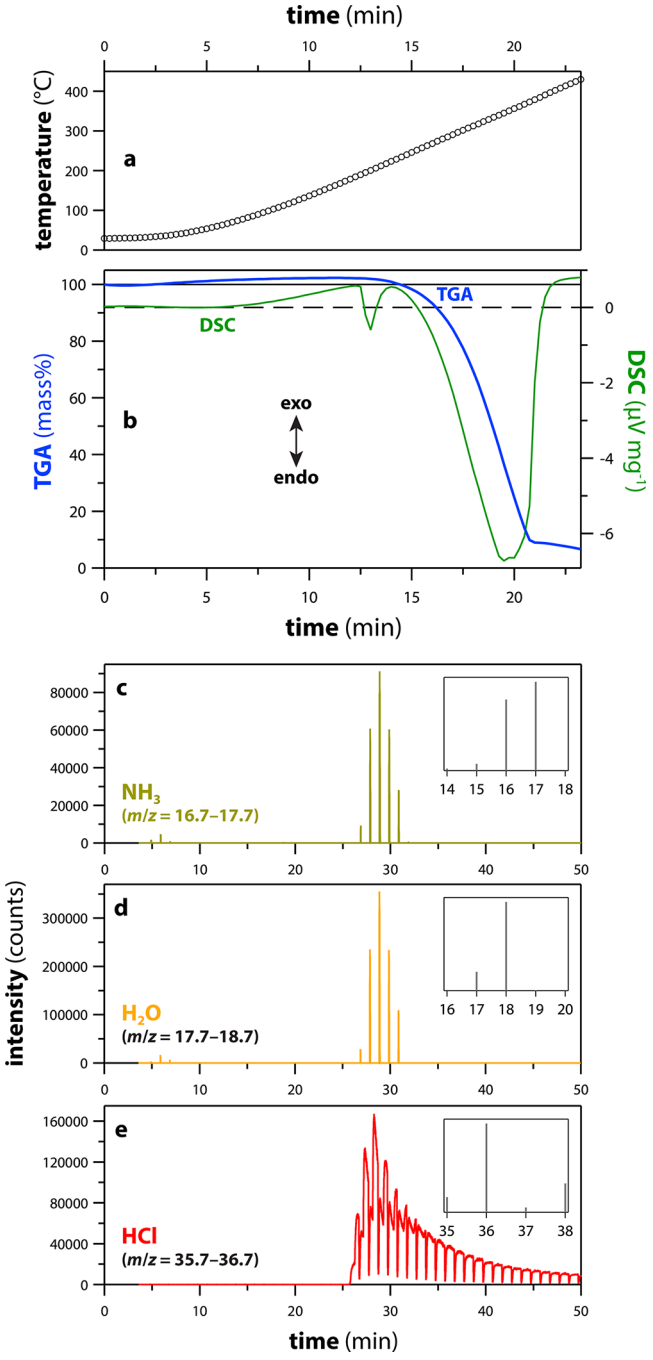

Figure 10. DSC-TGA-EGA data for NH_4Cl including (a) temperature vs time, (b) DSC-TGA data, (c) GC−MS data for NH_3, (d) GC−MS data for H_2O, and (e) GC−MS data for HCl. The data was shifted to show the GC−MS data aligned with the mass loss (TGA) curve. Insets on the GC−MS data show the mass spectra for each set of ions used to identify the species (i.e., intensity vs ion mass).

Second, the alumina crucibles used in these studies are susceptible to thermal shock (cracking) so heating or cooling them rapidly is a problem. Thus, finding a way to keep the dechlorinated melt at moderate temperatures (~600 °C) would be ideal to help prevent this from occurring, but that means that the other glass-forming chemicals (e.g., Fe_2O_3) would have to be charged into the crucible while the system is at these temperatures. One way to do this would be to insert the chemicals down the off-gas glassware to prevent contaminating the inside of the furnace, but this would mean contaminating the NH_4Cl with these chemicals. This is an engineering challenge that should be addressed and could potentially include the installation of a secondary system connected to the crucible snorkel on the crucible (Figure 2-c3), separate from the off-gas port, for charging chemicals into the crucible. Of course, if this were done, that port would have to remain plugged during dechlorination or it could fill, or even plug, with NH_4Cl condensates unless it was kept at high temperatures.

Another reason that this was not implemented has to do with the temperature limitations of coil heating elements, which are rated to 1150−1200 °C. Some of the phosphate glass formulations require vitrification temperatures in excess of these temperatures, making it difficult to successfully vitrify these formulations in this type of furnace setup. Alternate types of heating elements are available (e.g., $MoSi_2$) for achieving higher temperatures, but these pose additional challenges such as the way they are installed with electrical-bus connections on the top of the furnace chamber (where the current gradient furnace sits) and greater exposure to any potential NH_4Cl vapors (the current coil elements are less exposed) that might escape the crucible during the dechlorination process, potentially leading to corrosion of the elements.

Third, performing the vitrification step without cooling the dechlorinated melt would be a better way to achieve homogeneity in the vitrified product. The current approach is to put Fe_2O_3 powder on top of the solidified dechlorinated product. These two react well during vitrification, but it is common to see a small amount of unreacted Fe_2O_3 in the crucible after vitrification in some of the formulations.

Fourth, the G1DA and G2DA both comprised separate pieces composed of fused quartz or alumina. Neither of these construction materials are ideal from a scale-up perspective. The fused quartz is very fragile to handle and "frosts" (i.e., turns cloudy) over time when exposed to compounds containing chemicals like alkalis and halides. This frosting effect also makes the fused quartz more brittle over time. Also, alumina is not ideal as a crucible material due to the thermal shock susceptibility (described previously) because they are expensive to fabricate, they can only be used once, and they are very susceptible to corrosion by phosphate melts (i.e., all the vitrified products contain Al_2O_3 from the crucible). It should also be mentioned that iron phosphate glasses made in fused quartz crucibles are more durable than those made in alumina crucibles, suggesting that alumina could be negatively affecting these properties.[34] An ideal system, including both the crucible and off-gas lines, should be made of less reactive materials such as a metal alloy like Inconel 690 or 693. While these Inconel alloys have been demonstrated to work well for iron phosphate glasses,[40,41] it is unclear how they would perform with the dechlorination melts that have much lower melting temperatures (T_m < 600 °C) and very low viscosities.

Lastly, exploration of a cold finger system to highly concentrate the solid NH_4Cl condensates should be explored. It is possible that the condensates could be easily collected in this manner, without a flow-through-type solid-condensate-collection system in a separate chamber while the more volatile byproducts (e.g., H_2O, HCl, and NH_3) travel to a liquid condenser system like the ones employed in both the G1DA and G2DA designs. If something like this were implemented, then it is possible that the cold finger could be removed periodically for harvesting NH_4Cl and replaced with a clean cold finger for future condensate collections.

https://doi.org/10.1021/acsomega.1c05065
ACS Omega 2021, 6, 32239−32252

6. SUMMARY AND CONCLUSIONS

The generation-2 dechlorination apparatus worked much better than the generation-1 system at (1) preventing NH_4Cl from clogging the off-gas glassware using the same batch size, (2) controlling the temperature of the primary NH_4Cl condensation region (spread over 5.6−10.1 cm vs ∼3.1 cm) by utilizing the gradient furnace, and (3) preventing splattering of the melt onto the snorkel glassware. Having the NH_4Cl condensates spread across a wider region of the glassware helped with the NH_4Cl recovery process as well. For the KCl (G2DA Run-1) and CsCl (G2DA Run-2) experiments, the NH_4Cl recoveries were 83.4 and 85.4 mass %, respectively, which are much higher than those achieved in the G1DA, which were only 13.8 and 15.5 mass %, respectively. Thermodynamic measurements of (a) ADP + KCl and (b) NH_4Cl revealed that the temperatures utilized were successful at performing the expected reactions based on literature documentation of similar processes.

The changes in the generation-2 system drastically improved the process flow and should work well for scaling up the salt processing rate and throughput compared to the generation-1 system. Discussion was also provided to describe some changes that could be made in a future redesign if the generation-2 dechlorination apparatus was to be upgraded. These included (1) using a horizontal off-gas system design to help prevent NH_4Cl from falling into the crucible, (2) using a purge gas to drive condensates out of the furnace more effectively, (3) performing the vitrification step without cooling down the dechlorinated melt, (4) using different construction materials for the crucible and off-gas lines such as metal alloys instead of fused quartz and alumina, and (5) using a cold finger system to collect NH_4Cl condensates in a way that they are easier to recover for recycle.

■ ASSOCIATED CONTENT

Supporting Information

The Supporting Information is available free of charge at https://pubs.acs.org/doi/10.1021/acsomega.1c05065.

Process flow diagram of the dechlorination, vitrification, and NH_4Cl recycle processes; schematic of the generation-1 dechlorination apparatus; schematics of the generation-2 dechlorination apparatus; gradient furnace profiling plots; Sigmoid fitting parameters; thermal profiles used for dechlorination experiments; pictures of the condensates; and X-ray diffraction data (PDF)

■ AUTHOR INFORMATION

Corresponding Author

Brian J. Riley − *Pacific Northwest National Laboratory, Richland, Washington 99354, United States;* orcid.org/0000-0002-7745-6730; Email: brian.riley@pnnl.gov

Authors

Saehwa Chong − *Pacific Northwest National Laboratory, Richland, Washington 99354, United States;* orcid.org/0000-0002-4722-0022

Charmayne E. Lonergan − *Pacific Northwest National Laboratory, Richland, Washington 99354, United States*

Complete contact information is available at: https://pubs.acs.org/10.1021/acsomega.1c05065

Funding

This work was supported by the DOE Office of Nuclear Energy's Nuclear Technology Research and Development (NTRD) Program under the Material Recovery and Waste-form Development (MRWFD) Campaign.

Notes

The authors declare no competing financial interest.

■ ACKNOWLEDGMENTS

Pacific Northwest National Laboratory is operated by Battelle Memorial Institute for the DOE under contract DE-AC05-76RL01830. The authors thank Kimberly Gray of DOE-NE and Ken Marsden at Idaho National Laboratory for their support and programmatic guidance. The authors express thanks to JJ Stevenson at Deltech, Inc. for helping in designing and fabricating the furnace and to Joelle Reiser for helpful comments on the manuscript.

■ REFERENCES

(1) Williamson, M. A.; Willit, J. L. Pyroprocessing flowsheets for recycling used nuclear fuel. *Nucl. Eng. Technol.* **2011**, *43*, 329.

(2) LeBlanc, D. Molten salt reactors: A new beginning for an old idea. *Nucl. Eng. Des.* **2010**, *240*, 1644.

(3) Riley, B. J.; McFarlane, J.; DelCul, G. D.; Vienna, J. D.; Contescu, C. I.; Forsberg, C. W. Molten salt reactor waste and effluent management strategies: A review. *Nucl. Eng. Des.* **2019**, *345*, 94.

(4) Vance, E. R.; Davis, J.; Olufson, K.; Chironi, I.; Karatchevtseva, I.; Farnan, I. Candidate waste forms for immobilisation of waste chloride salt from pyroprocessing of spent nuclear fuel. *J. Nucl. Mater.* **2012**, *420*, 396.

(5) Chong, S.; Riley, B. J.; Asmussen, R. M.; Lawter, A. R.; Bruffey, S. H.; Nam, J.; McCloy, J. S.; Crum, J. V. Iodosodalite synthesis with hot isostatic pressing of precursors produced from aqueous and hydrothermal processes. *J. Nucl. Mater.* **2020**, *538*, 152222.

(6) Chong, S.; Peterson, J. A.; Riley, B. J.; Tabada, D.; Wall, D.; Corkhill, C. L.; McCloy, J. S. Glass-bonded iodosodalite waste form for immobilization of ^{129}I. *J. Nucl. Mater.* **2018**, *504*, 109.

(7) Riley, B. J.; Vienna, J. D.; Frank, S. M.; Kroll, J. O.; Peterson, J. A.; Canfield, N. L.; Zhu, Z.; Zhang, J.; Kruska, K.; Schreiber, D. K.; Crum, J. V. Glass binder development for a glass-bonded sodalite ceramic waste form. *J. Nucl. Mater.* **2017**, *489*, 42.

(8) Yao, T.; Lu, F.; Sun, H.; Wang, J.; Ewing, R. C.; Lian, J. Bulk iodoapatite ceramic densified by spark plasma sintering with exceptional thermal stability. *J. Am. Ceram. Soc.* **2014**, *97*, 2409.

(9) Cao, C.; Chong, S.; Thirion, L.; Mauro, J. C.; McCloy, J. S.; Goel, A. Wet chemical synthesis of apatite-based waste forms - A novel room temperature method for the immobilization of radioactive iodine. *J. Mater. Chem. A* **2017**, *5*, 14331.

(10) Macerata, E.; Pizzi, E.; Ossola, A.; Giola, M.; Mariani, M. Fluorapatite as immobilization matrix for nuclear waste. *Radiat. Eff. Defects Solids* **2018**, *173*, 763.

(11) Riley, B. J.; Pierce, D. A.; Crum, J. V.; Williams, B. D.; Snyder, M. M. V.; Peterson, J. A. Waste form evaluation for $RECl_3$ and REO_x fission products separated from used electrochemical salt. *Prog. Nucl. Energy* **2018**, *104*, 102.

(12) Lee, C. W.; Pyo, J.-Y.; Park, H.-S.; Yang, J. H.; Heo, J. Immobilization and bonding scheme of radioactive iodine-129 in silver tellurite glass. *J. Nucl. Mater.* **2017**, *492*, 239.

(13) Riley, B. J. Electrochemical salt wasteform development: A review of salt treatment and immobilization options. *Ind. Eng. Chem. Res.* **2020**, *59*, 9760.

(14) Riley, B. J.; Peterson, J. A.; Vienna, J. D.; Ebert, W. L.; Frank, S. M. Dehalogenation of electrochemical processing salt simulants with ammonium phosphates and immobilization of salt cations in an iron phosphate glass waste form. *J. Nucl. Mater.* **2020**, *529*, 151949.

(15) Lee, K. R.; Riley, B. J.; Park, H.-S.; Choi, J.-H.; Han, S. Y.; Hur, J.-M.; Peterson, J. A.; Zhu, Z.; Schreiber, D. K.; Kruska, K.; Olszta, M. J. Investigation of physical and chemical properties for upgraded SAP (SiO_2-Al_2O_3-P_2O_5) waste form to immobilize radioactive waste salt. *J. Nucl. Mater.* **2019**, *515*, 382.
(16) Park, H.-S.; Cho, I.-H.; Eun, H. C.; Kim, I.-T.; Cho, Y. Z.; Lee, H.-S. Characteristics of wasteform composing of phosphate and silicate to immobilize radioactive waste salts. *Environ. Sci. Technol.* **2011**, *45*, 1932.
(17) Gardner, L.; Wasnik, M.; Riley, B.; Simpson, M.; Carlson, K. Effect of reduced dehalogenation on the performance of Y zeolite-based sintered waste forms. *J. Nucl. Mater.* **2021**, *545*, 152753.
(18) Wasnik, M. S.; Grant, A. K.; Carlson, K.; Simpson, M. F. Dechlorination of molten chloride waste salt from electrorefining via ion-exchange using pelletized ultra-stable H-Y zeolite in a fluidized particle reactor. *J. Radioanal. Nucl. Chem.* **2019**, *320*, 309.
(19) National Research Council *Glass as a Waste Form and Vitrification Technology: Summary of an International Workshop*; The National Academies Press: National Research Council: Washington, DC, 1996.
(20) Jantzen, C. M. Development of glass matrices for high level radioactive wastes. In *Handbook of Advanced Radioactive Waste Conditioning Technologies*; Ojovan, M. I., Ed.; Woodhead Publishing Series in Energy: Oxford, 2011, p 230, DOI: 10.1533/9780857090959.2.230.
(21) Kim, C.-W.; Day, D. E. Immobilization of Hanford LAW in iron phosphate glasses. *J. Non-Cryst. Solids* **2003**, *331*, 20.
(22) Kim, C. W.; Ray, C. S.; Zhu, D.; Day, D. E.; Gombert, D.; Aloy, A.; Moguš-Milanković, A.; Karabulut, M. Chemically durable iron phosphate glasses for vitrifying sodium bearing waste (SBW) using conventional and cold crucible induction melting (CCIM) techniques. *J. Nucl. Mater.* **2003**, *322*, 152.
(23) Schlenz, H.; Heuser, J.; Neumann, A.; Schmitz, S.; Bosbach, D. Monazite as a suitable actinide waste form. *Z. Kristallogr.* **2013**, *228*, 113.
(24) Boatner, L. A.; Beall, G. W.; Abraham, M. M.; Finch, C. B.; Huray, P. G.; Rappaz, M., Monazite and other lanthanide orthophosphates as alternate actinide waste forms. In *Advances in Nuclear Science & Technology*; Northrup, Jr., C. J. M., Ed. 1980, p 289.
(25) McCarthy, G. J.; White, W. B.; Pfoertsch, D. E. Synthesis of nuclear waste monazites, ideal actinide hosts for geologic disposal. *Mater. Res. Bull.* **1978**, *13*, 1239.
(26) Donze, S.; Montagne, L.; Palavit, G. Thermal conversion of heavy metal chlorides ($PbCl_2$, $CdCl_2$) and alkaline chlorides (NaCl, KCl) into phosphate glasses. *Chem. Mater.* **2000**, *12*, 1921.
(27) Siemer, D. D. Improving the integral fast reactor's proposed salt waste management system. *Nucl. Technol.* **2012**, *178*, 341.
(28) Park, H.-S.; Kim, I.-T.; Cho, Y.-Z.; Eun, H.-C.; Lee, H.-S. Stabilization/solidification of radioactive salt waste by using $x SiO_2$–$y Al_2O_3$–$z P_2O_5$ (SAP) material at molten salt state. *Environ. Sci. Technol.* **2008**, *42*, 9357.
(29) Pardo, A.; Romero, J.; Ortiz, E. High-temperature behaviour of ammonium dihydrogen phosphate. *J. Phys.: Conf. Ser.* **2017**, *935*, No. 012050.
(30) Wiberg, E.; Wiberg, N. *Inorganic Chemistry*; Academic Press, 2001.
(31) Herrmann, S. D. Memorandum to JC Price; Experiment Plan for Ternary Salt Synthesis with Mark IV Electrorefiner Uranium Dendrites in FCF. *Personal communication*.
(32) Gardner, L. D.; Wasnik, M. S.; Riley, B. J.; Chong, S.; Simpson, M. F.; Carlson, K. L. Synthesis and characterization of sintered H-Y zeolite-derived waste forms for dehalogenated electrorefiner salt. *Ceram. Int.* **2020**, *46*, 17707.
(33) Riley, B. J.; Kroll, J. O.; Peterson, J. A.; Pierce, D. A.; Ebert, W. L.; Williams, B. D.; Snyder, M. M. V.; Frank, S. M.; George, J. L.; Kruska, K. Assessment of lead tellurite glass for immobilizing electrochemical salt wastes from used nuclear fuel reprocessing. *J. Nucl. Mater.* **2017**, *495*, 405.
(34) Riley, B. J.; Chong, S. Effects of composition and canister centerline cooling on microstructure, phase distribution, and chemical durability of dehalogenated iron phosphate waste forms. *submitted to the J. Non-Cryst. Solids* **2021**.
(35) Ebert, W. L.; Fortner, J. A. *Corrosion Behavior of Developmental Iron Phosphate Glass Waste Forms*; ANL/CFCT-20/1, Argonne National Laboratory: Lemont, IL, 2020.
(36) Ebert, W. L.; Fortner, J. A. *Corrosion Tests with Developmental Iron Phosphate Glass Waste Forms*; ANL/CFCT-19/7, Argonne National Laboratory: Lemont, IL, 2019.
(37) Ebert, W. L.; Fortner, J. A. *Analyses of Iron Phosphate Glasses for Dehalogenated Salt Waste*; ANL/CFCT-19/5, Argonne National Laboratory: Lemont, IL, 2019.
(38) Vainshtein, B. K. Refinement of the structure of the group NH_4 in the structure of ammonium chloride. Trudy Instituta Kristallografii, Akademiya Nauk SSSR 1956, *12*, 18.
(39) *CRC Handbook of Chemistry and Physics*; 88th ed.; CRC Press: Boca Raton, FL, 2007–2008.
(40) Hsu, J.-H.; Newkirk, J. W.; Kim, C.-W.; Ray, C. S.; Brow, R. K.; Schlesinger, M. E.; Day, D. E. Corrosion of Inconel 690 and Inconel 693 in an iron phosphate glass melt. *Corros. Sci.* **2013**, *75*, 148.
(41) Hsu, J.-H.; Newkirk, J. W.; Kim, C.-W.; Brow, R. K.; Schlesinger, M. E.; Ray, C. S.; Day, D. E. The performance of Inconel 693 electrodes for processing an iron phosphate glass melt containing 26wt.% of a simulated low activity waste. *J. Nucl. Mater.* **2014**, *444*, 323.

https://doi.org/10.1021/acsomega.1c05065
ACS Omega 2021, 6, 32239–32252